Eurotherm Seminar #99
Advances in Thermal Energy Storage

EUROTHERM99-01-074

Numerical analysis of natural convection in a latent heat thermal energy storage system containing rectangular enclosures

Julian Vogel, Maike Johnson, Markus Eck, Dörte Laing

German Aerospace Center (DLR), Pfaffenwaldring 38-40, Stuttgart, Germany, Phone: 49-711-6862 469, Fax: 49-711-6862 747, e-mail: julian.vogel@dlr.de

1. Abstract

Natural convection in the liquid phase of a phase change material (PCM) is often neglected in the analysis and design of latent heat thermal energy storage (LHTES) systems. However, depending on geometry and material properties, the influence of natural convection can be significant. This is also the case in an experimental LHTES lab-scale storage unit for high temperature PCMs that was designed, built and operated at DLR. The unit is a storage adaptation of a flat plate heat exchanger. The space between the heated flat plates forms rectangular enclosures, which are filled with PCM. The behavior of such a system is to be described by numerical methods. First, a method that accounts only for heat conduction was used. In some cases, simulated results diverged considerably from experimental data. This divergence was expected to be mostly caused by natural convection. In this work, improved simulation methods are applied that include the modeling of natural convection. For a detailed reference solution, a sophisticated CFD-Method that solves the Navier-Stokes-Equations is used. The results are validated with data from the above mentioned DLR storage test unit filled with the eutectic mixture of potassium nitrate (KNO_3) and sodium nitrate ($NaNO_3$). Although differences between simulation results and experimental data still remain, the agreement has improved greatly in comparison to previous heat conduction simulations. Possible causes for divergences and suggestions for further improvement are given. Moreover, the detailed flow and temperature fields driven by natural convection are presented and discussed. Finally, the influence of natural convection on the thermal power characteristic is analyzed. A strong influence is observed for the charging process, where the power input is considerably enhanced. The discharging process is only slightly affected.

Keywords: Latent heat thermal energy storage; phase change material (PCM); solidification and melting; natural convection; rectangular enclosures; numerical simulation (CFD);

2. Introduction

Thermal energy storage (TES) systems can be applied whenever there is a mismatch between supply and demand of thermal energy. When thermal energy is stored in the latent heat of a phase change material (PCM), the system is a latent heat thermal energy storage (LHTES). There are various concepts for transferring heat into and out of the storage with various system parameters. The various system parameters relate to various applications for the storages. An overview of the topic is given by Mehling and Cabeza [1]. Thermal energy storage systems can be roughly classified by the temperature range in which heat is to be stored, the storage capacity and the heat transfer fluid (HTF), by which heat is transferred into and out of the storage.

In this work, a flat plate heat exchanger-type system for high temperature storage is investigated. The HTF flows through flat plates and the PCM is contained in rectangular enclosures between them. The PCM used is a mixture of potassium nitrate (KNO_3) and sodium nitrate ($NaNO_3$) that melts at 219.5 °C. The latent storage capacity with this PCM is approximately 7.5 kWh. Thermal oil is used as HTF for the experimental test runs. Common applications for this system are industrial processes.

Simulations of the system have already been performed using a heat conduction model. However, results deviated from experimental data and the influence of natural convection was considered likely as a major reason for the discrepancy. Numerical simulations that account for natural convection in a PCM contained in a rectangular enclosure have been performed by various authors for different dimensions and materials. An example is an extensive study on a paraffin wax in relatively small enclosures by Shatikian, Ziskind, Letan et al. [4]. However, there is no study of larger enclosures with high aspect ratios or nitrate salts as PCM so far. Furthermore, numerical investigations are often not validated by experimental data. In this work, the impact of natural convection in a large enclosure with high aspect ratio filled with a nitrate salt as PCM is simulated. The results are compared to data from the experimental storage unit.

In the following, the storage system is characterized and the mechanisms of heat transfer occurring in PCM storages are discussed.

2.1. Characterization of the experimental storage unit

The type of geometry addressed in this study is a small scale prototype of a flat plate heat exchanger that was specifically designed for thermal energy storage by Fiss [2]. The design is described by Johnson, Fiss, Klemm et al. [3] and is illustrated in Figure 1. The system is designed for operating temperatures up to 300°C. It contains rectangular enclosures filled with PCM that are open to the atmosphere (PCM chambers). This initial storage unit for testing purposes is comprised of two outer, smaller PCM chambers to reduce the impact of environmental heat losses on the two inner, wider PCM chambers used for analysis. In this setup, the PCM is heated or cooled by the thermal oil Mobiltherm 603 as the heat transfer fluid (HTF). It flows through oil chambers in three flat plates between the PCM chambers and is transferred to or from the energy drain or source, respectively, by two outlet/inlet flanges. The storage unit is integrated in a heating/cooling loop at the DLR lab facilities in Stuttgart with a maximum flow rate of 3 m³/h, a heating power of 12 kW and a cooling power of 30 kW.

The open chamber design of the storage allows for an adjustment of the transferred heat rate by the insertion of heat transfer structures. The storage can thereby be adapted to different application requirements. Various structure geometries were considered and analyzed [3]. However, for the validation of the simulation model, only the PCM chambers without heat transfer structures are analyzed.

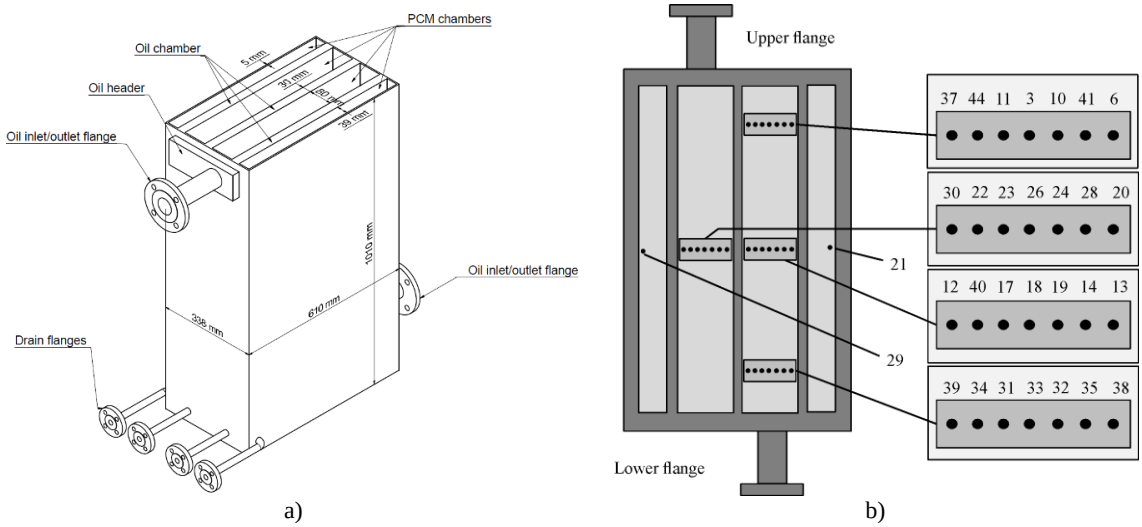

Figure 1: Illustration of the experimental storage unit and arrangement of thermocouples in the PCM chambers

During experimental testing, temperatures are measured at the HTF inlet and outlet and at different positions at half of the vertical height in the PCM chambers. The distribution of measurement positions in the PCM chambers is depicted in Figure 1 b). In one of the middle chambers, temperatures are measured at three different positions over the length of the chamber. For comparison, the middle position is also measured in the other wide PCM chamber. At each of these positions, seven thermocouples are fixated in metal plates over the width of the chamber. The distance between measurement points per plate is 10 mm. Two additional measurement points are in the outer PCM chambers.

2.2. Heat transfer mechanisms in latent heat thermal energy storages

The heat transfer into and out of a LHTES is a problem of conjugate heat transfer, in which four different regions can be identified: forced convection in the heat transfer fluid, conduction in the solid containment, conduction in the solid PCM and either conduction or natural convection in the liquid PCM. The occurrence and magnitude of natural convection is due to density gradients in the liquid and depends on material properties, boundary conditions and geometrical dimensions, which is described for example in the experimental work by Elder [5].

Especially during the charge process, the effect of natural convection is significant. In this case, a temperature difference between the heated wall and the melting front prevails until the entire solid is melted. Instead, during discharge, the PCM solidifies at the cold wall and the temperature difference between the solidification front and the remaining liquid vanishes quickly. Natural convection occurs only in a short period of time until the whole liquid is cooled to its solidification temperature. In the solidified PCM, heat transfer occurs only by conduction.

3. Materials and method

The aim of this work is to analyze the impact of natural convection during the melting and solidification processes of a PCM for the described LHTES unit by numerical means. First, the properties of the utilized materials are shown. Then, the geometry and its boundary conditions are described. Finally, the numerical method is presented.

3.1. Material data

The PCM used as storage material is a eutectic mixture of potassium nitrate and sodium nitrate (KNO_3-$NaNO_3$). The ratio of potassium nitrate to sodium nitrate is 54:46 wt. %. The melting temperature T_m of this mixture would theoretically be 222°C. However, for the technical grade material used in the experiments, the onset of melting was measured at a temperature of 219.15°C. With this material, the latent heat capacity of the storage system is approximately 7.5 kWh. The containment material is carbon steel 1.0425. Some relevant data of material properties are shown in Table 1, where ρ is the density, c is the specific heat capacity, k is the thermal conductivity, ΔH_m is the specific latent heat, β is the volumetric thermal expansion coefficient and μ is the dynamic viscosity. The material properties of the KNO_3-$NaNO_3$ mixture are given in the solid and liquid state at a temperature near the melting temperature.

Table 1: Thermophysical material properties

Material	ρ / kg m^{-3}	c / J (kgK)$^{-1}$	k / W (mK)$^{-1}$	T_m / °C	ΔH_m / kJ kg^{-1}	β / K^{-1}	μ / m^{2}s^{-1}
Steel 1.0425	7800	540	51	-	-	-	-
KNO_3-$NaNO_3$	2050 (s) 1959 (l)	1350 (s) 1492 (l)	0.457 (s) 0.435 (l)	219.5	108	$3.5 \cdot 10^{-4}$	$5.8 \cdot 10^{-3}$

3.2. Definition of simplified enclosure geometry and its boundary conditions

For the thermal analysis incorporating natural convection in the LHTES system, the geometry of the experimental unit, see Figure 1 a), is simplified by consideration of symmetries. The domain is reduced to the half of a PCM chamber and the inner wall of the adjacent flat plate filled with the HTF. The resulting simplified geometry is illustrated in Figure 2 a). In this three-dimensional space, the two-dimensional plane in the middle of the chamber is simulated. In the case of a rectangular container with a high aspect ratio of length L to depth D, a two-dimensional approximation is quite reasonable. The simulated domain lies in a plane spanned by the middle row of the thermocouples with numbers 12, 40 17, 18, see Figure 1 b).

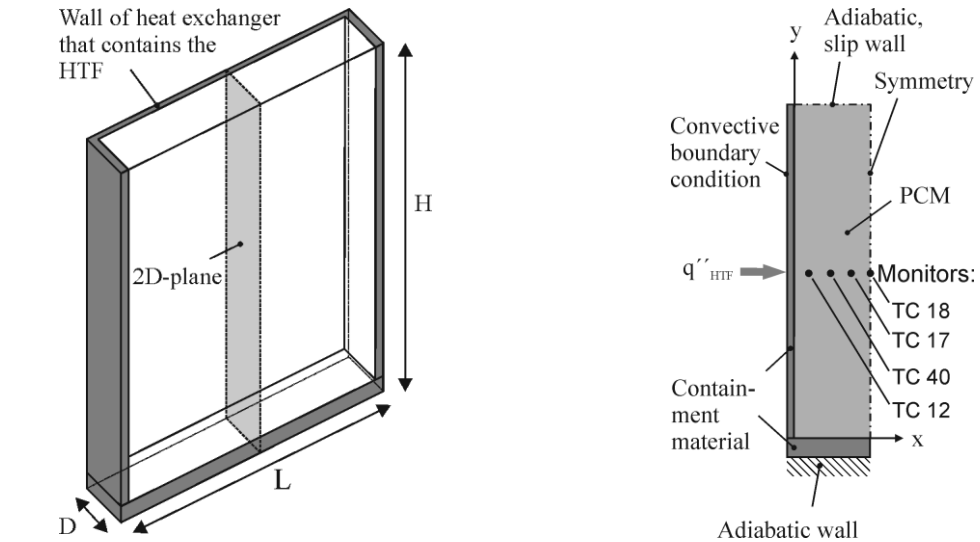

a) Simplified domain that results from symmetries b) Two-dimensional plane

Figure 2: Enclosure geometry and boundary conditions

The geometry of the simulated 2D plane and the applied boundary conditions are shown in Figure 2 b). The total depth and height including walls are $D = 42$ mm and $H = 1010$ mm; the dimensions of the PCM only are $D_{PCM} = 38$ mm and $H_{PCM} = 1000$ mm.

On the left side, a convective boundary condition is applied. The heat transfer rate per area into the domain is given by

$$q''_{HTF} = -\alpha \; T_W - T_{HTF} \; . \tag{1}$$

This is dependent on the heat transfer coefficient α, the temperature at the wall of the steel containment T_W and the temperature T_{HTF} in the heat transfer fluid, which is assumed to be constant over the height. However, in the experiment, the temperature T_{HTF} varies over time. During the charging process, T_{HTF} rises gradually due to the finite mass flow and limited heating power of the heating loop. During discharge, the cooling power is higher and heat losses are in favor of the process. In this case, the assumption of a constant temperature T_{HTF} is reasonable. The values derived from experimental data [3] are given in Table 2 as they are used in the simulations. The heat transfer coefficient is set to a constant value of $\alpha = 200 \frac{\mathrm{W}}{\mathrm{m^2 K}}$, which was also determined by experiments [3].

Table 2: Convective boundary condition temperature variation with time $T_{HTF}(t)$ while charging and discharging

t /s	0	2000	5000	11000	28800
T_{HTF} t while charging /°C	197	225	240	247	247
T_{HTF} t while discharging /°C	197	197	197	197	197

On the right side of the domain, see Figure 2 b), a symmetry boundary condition is applied that defines all gradients in the x-direction to be zero. On the top, where a layer of air and insulation follows, an adiabatic boundary condition with allowed slippage is defined. The insulated bottom of the base plate is assumed to be adiabatic due to relatively low heat losses. The monitor points, at which temperatures are evaluated in the simulations, are also shown in Figure 2 b).

3.3. Numerical Method

The previously described two-dimensional plane was simulated using a CFD-Method that solves the temperature field and the flow field. Natural convection is thereby incorporated by the motion of the fluid. The CFD simulations were performed in Fluent©, the geometry and mesh were built in ICEM CFD©, both from the ANSYS© package version 14.5.
For the results discussed in the next section, a structured mesh with two solid and one liquid zone was used. Different meshes have been built and compared to find an optimum of accuracy and calculation time. A mesh with an adaptive grid refinement at the phase front was also used. Calculations using this grid resulted in a wavy phase front, which was not seen in much finer grids. Hence, the adaptive grid was thought to influence the results in an adverse fashion. The final mesh used has a medium resolution with a total number of 55188 quadrilateral control volume elements. It is refined at the walls with a minimum distance of 0.2 mm to allow for a correct boundary layer development. Further from the walls, the cell size is coarsened to reduce the total cell count. The maximum cell size is restricted to 1 mm in both dimensions to maintain a sufficient resolution of the phase front. The simulation time step was chosen to be preferably large, but still fits the mesh and leads to fast convergence with a value of 0.5 s.
For the simulation of heat conduction, only the energy equation is solved. To implement natural convection, the equations of continuity, momentum and energy are solved. The Boussinesq approximation is used, which treats the density ρ as a constant value ρ_0 in all equations. Density gradients are included only in the buoyancy term in the vertical momentum equation. According to the Fluent manual [6], this term is simplified as follows:

$$\rho - \rho_0 \; g \approx -\rho_0 \beta \; T - T_0 \; g. \tag{2}$$

Here, β is the volumetric expansion coefficient as given in Table 1 and T_0 is the operating temperature, at which the density ρ_0 prevails. Regarding natural convection in the liquid, this approximation is reasonable and common. However, the discontinuous density during solidification and melting can not be taken into account. Hence, volumetric expansion is not possible in this model. The remaining material properties are also set to constant; for the

charging process to the value of the solid state and for the discharging process to the value of the liquid state, see Table 1. This simplifies the model and results in better convergence of the governing equations. The resulting deviations are considered to be rather small. To incorporate the phase transition of the PCM, the "solidification and melting" model implemented in Fluent is used. With it, the energy equation is modified via the enthalpy method by Voller and Prakash [7]. To allow for gradual flow acceleration in the region between the liquid and solid state, the model uses the enthalpy-porosity technique as described by Brent, Voller and Reid [8].
For every time step, iterations continue until certain criteria of the residuals of the governing equations are fulfilled. The continuity equation and the momentum equations are converged, when a scaled residual of 10^{-3} is reached. The energy equation is converged, when a scaled residual of 10^{-9} is reached.

4. Results and discussion

The results from a model that simulates heat transfer by conduction only and the detailed simulations including natural convection are discussed and compared to experimental data. Moreover, the melting process during charging with the natural convection model is discussed. At last, the input and output of thermal power is compared between the two models.

4.1. Conduction model compared to experimental data

Results from two-dimensional simulations with the conduction heat transfer model compared to experimental data from the described experimental storage unit are shown in Figure 3. Two of the thermocouples of the experiment are evaluated; TC12 is near the wall and TC18 in the middle of the PCM chamber, see Figure 1 b). During the initial charge process, simulation results correspond well to experimental data. But after approximately 9000 s, the measurement data suddenly rises steeply and approaches the charging temperature. This behavior can be explained by the onset of natural convection. Simulated values, on the other hand, remain constant for TC18 until 21600 s passed. In the discharge process, a deviation in the trend is seen from the beginning. The simulated temperature at TC18 sinks slower than in the experiment in the first 7200 s. However, the following isothermal melting process is correctly represented. Finally, after solidification is finished in the experiment, the simulated temperature at TC18 again remains higher for quite a large period. In summary, the simulated temperatures deviate significantly from the experiment while charging and only slightly while discharging. The deviation is considered likely to be by natural convection in the experiment.

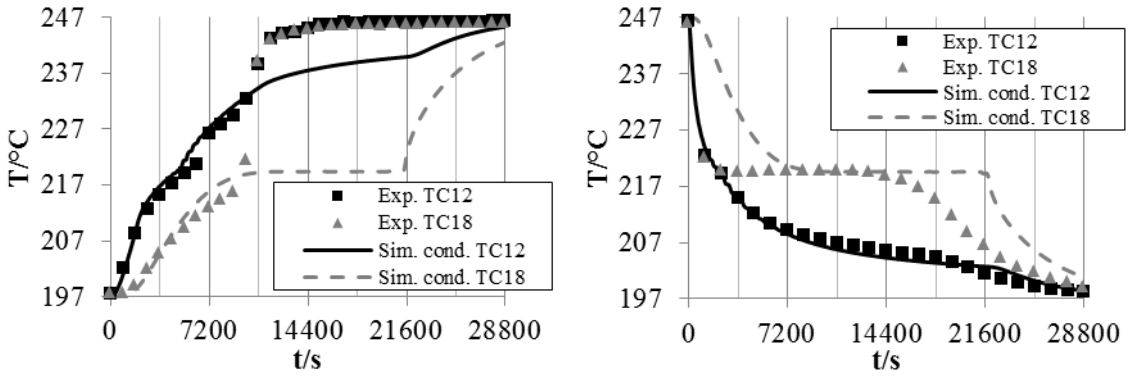

a) Charging process with T_{HTF} t $= 197 \ldots 247°C$ b) Discharging process with $T_{HTF} = 197°C$

Figure 3: Comparison of temperature progression over time between experimental and conduction heat transfer simulation results for the a) charging process and b) discharging process. Symbols represent experimental values from thermocouples TC12 and TC18, see Figure 1 b), lines are from the simulations evaluated at the same positions.

4.2. Natural convection model compared to experimental data

The results obtained from the detailed CFD simulations are also first compared to experimental data. Temperatures are plotted over time in Figure 4 for the a) charging process and b) discharging process. Again temperatures of the two thermocouples TC12 and TC18 are examined. During the charging process, the time until the melting front reaches the point TC18 decreases with natural convection compared to the conduction simulation. The simulated temperatures are now in good agreement with the experiment. At the beginning of the discharge process, simulated temperatures correspond to the experimental data well. Because of the strong heat transfer by natural convection in the liquid, they are nearly equal at both positions as long as the surrounding PCM is liquid. The time until the PCM solidifies at position TC18 reduces slightly in the simulation with natural convection compared to the conduction simulation and converges toward the experimental data. However, in the experiment, the temperature at TC18 falls earlier below the melting temperature and decreases gradually. In contrast, the simulated temperature TC18 remains at melting temperature longer and then sinks with a steep slope. This indicates a solidification behavior that does not completely match between simulations and experiments.

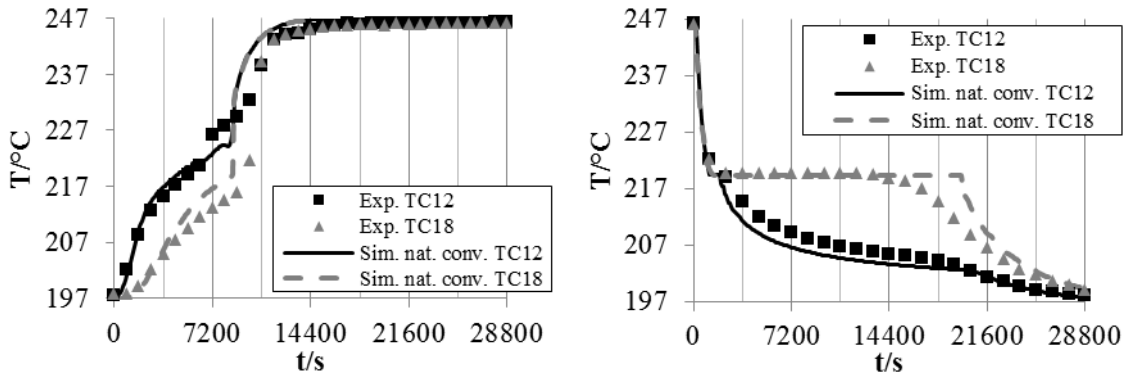

a) Charging process with T_{HTF} t $= 197 \ldots 247$°C b) Discharging process with $T_{HTF} = 197$°C

Figure 4: Comparison of temperature progression over time between the experiment and a simulation with heat transfer by natural convection for the a) charging and b) discharging process. Symbols represent experimental values from thermocouples TC12 and TC18, see Figure 1 b), lines are from simulations evaluated at the same positions.

Despite the improved qualitative and quantitative representation, the simulations still show a qualitative difference to experimental data at the end of the discharge process. One reason for this may be the excluded heat losses. Moreover, the positions of the thermocouples may not match exactly with the ideally assumed positions in the simulations. Also, measurements in convection regimes may be influenced by the thermocouples immersed in the flow field. Additionally, thermocouples can not measure an exact position; they rather measure the temperature over the length of a certain distance from the tip. Deviations may also arise from physical effects that are not included in the simulations. There are the effect of volume change due to phase change, the air phase directly above the upper PCM surface and variable material properties. Furthermore, the boundary conditions are modeled uniformly. For example, the temperature in the HTF is constant over the height of the flat plate, while in reality there is a vertical temperature gradient in the wall.

4.3. Detailed discussion of the melting process during charging

Despite the small remaining differences between simulations and experiments, the simulation model is validated by the experiment to have a sufficient accuracy. Hence, the detailed simulation results offer further insight into the physical behavior of the storage system. The time dependent liquid fraction and temperature fields for the charging process are depicted in Figure 5. In the beginning, for small widths of the liquid layer, heat transfer is dominated by

conduction. The melting front is mostly vertical and the temperature gradient is horizontal at 3600 s. With an increasing width of the liquid layer at 5400 s, natural convection becomes greater and hot fluid is transported to the upper part of the PCM, where melting is amplified. The PCM then starts to melt from top to bottom, which is seen from 7200 s to 10800 s. Finally, only a small solid piece is left at 13500 s. Normally, the solid PCM would gradually sink, but the possibility of solid parts moving in a liquid surrounding is not implemented in the model. If the solid would permanently lie on the bottom plate, the rate of melting would be increased. An important fact from the detailed simulations is that the time until complete melting can not be determined by thermocouples that are not directly above the bottom plate. Due to the melting from top to bottom, the thermocouples in the experiment at a height of 0.5 m detect melting when there is still solid PCM below them. In the CFD simulations, 14200 s pass until the complete PCM is melted. In comparison, melting at position TC18 occurs after 8800 s.

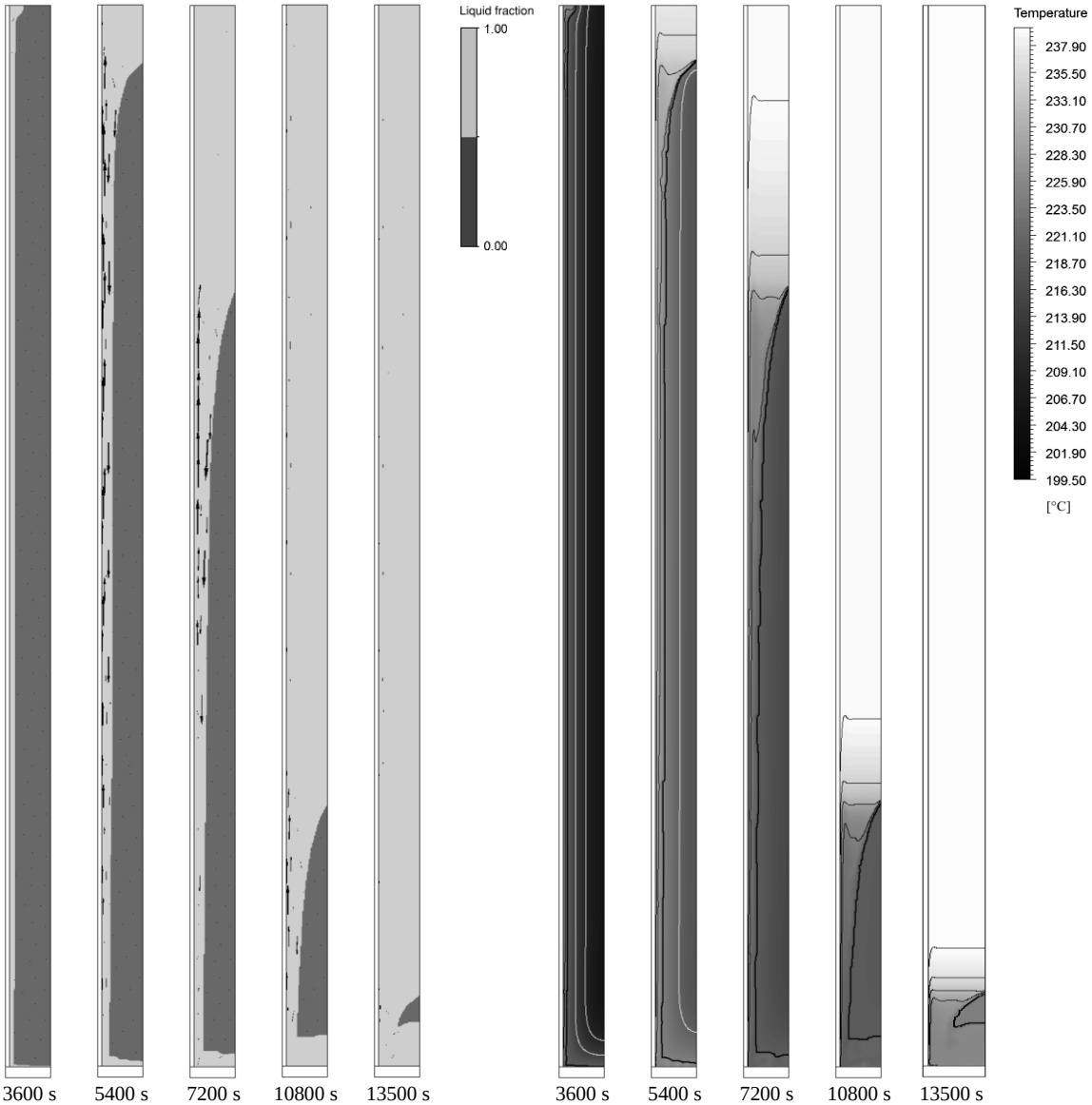

a) Liquid fraction and velocity vectors b) Temperature contours and isotherms

Figure 5: Time progression for the charging test case of a) liquid fraction and velocity vectors and b) contours and isotherms of temperature. The liquid fraction field shows two contours with light grey (liquid) and dark grey (solid) as well as velocity vectors. The temperature field is described by a contour plot ranging from $T = 199.5$°C (black) to $T = 239.5$°C (white). Several isotherms are highlighted. The thick black line depicts the melting temperature $T_m = 219.5$°C, the thin isotherms are above (black) or below (white) with steps of 5 K.

4.4. Impact of natural convection on thermal power

The thermal power transferred into and out of the storage, respectively, is examined here more thoroughly. In Figure 6, the results obtained from natural convection simulations are compared to those with conduction only. As expected, the power is only affected significantly during charging. In this case, after about an hour, the convection mechanism strongly increases the power input until a time of 4700 s. Then, the rise of thermal power by convection is slowed down due to the reduced area participating in heat transfer with a diminishing height of solid material. From the isotherms in Figure 5, it is seen that heat is only transferred over that height where there is still solid material. In the discharge case, the power output is similar with the conduction and natural convection model. At a closer look, the power is somewhat higher in the first half hour in the natural convection model, but then its impact vanishes and the power is even a little lower due to the already explained effect of the reduced effective heat transfer area.

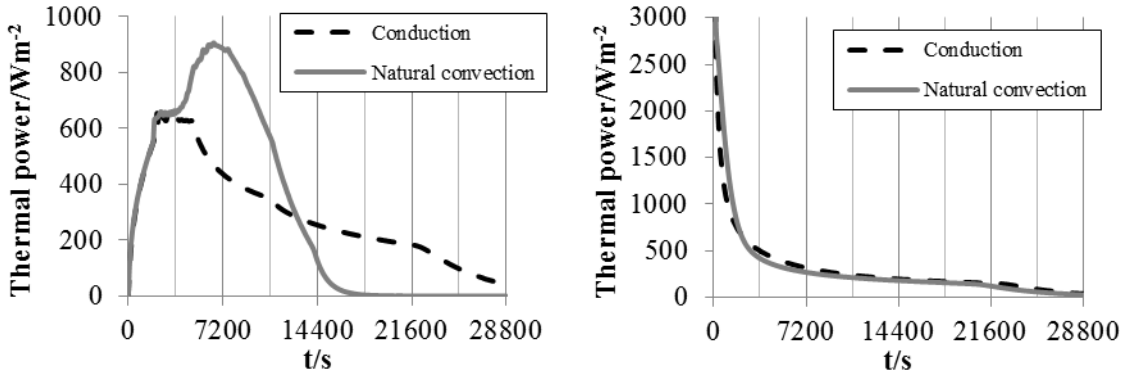

a) Charging process b) Discharging process

Figure 6: Comparison of thermal power output/input progression over time between the simulation with conduction only and that with natural convection for the a) charging process and b) discharging process.

5. Conclusions

The presented modelling approach with a CFD method that incorporates natural convection offers improved results compared to conduction only calculations. However, discrepancies with experimental data still remain. Especially during discharge, the experimentally measured temperature farthest away from the cooled wall solidifies considerably sooner with a gradual temperature decrease, while in the simulation, the temperature sinks later and with a steep slope. Among the possible reasons are heat losses that were not accounted for in the simulation, the influence of the thermocouples immersed in the PCM on the measurements and physical effects not included in the simulation model. Detailed simulation results of the charge process, namely the fields of liquid fraction and temperature give further insight into the melting mechanism. They indicate the expected convex deformation of the phase front and the vertical temperature gradient. In an enclosure with such a high aspect ratio, melting occurs explicitly from top to bottom. At last, thermal power input and output while charging and discharging, respectively, was illustrated and compared for both models. In the melting process during charging, thermal power is strongly increased after a certain time when the liquid layer is thick enough to allow for natural convection. However, when the melting front reaches the midplane on top, thermal power is again limited by the reduced effective heat transfer area. In the solidification process during discharging, thermal power is very similar between conduction and natural convection simulations.

To further improve the simulation model, heat losses determined from the experiment should be included. Also, the physics of melting and freezing may be enhanced by allowing a change of thermophysical material properties due to phase change. However, a change in density, and

hence volume, results in a significantly increased model complexity. To allow for a change in volume, the air phase above the PCM must also be simulated with another multiphase model, which leads to increased simulation costs. Another enhancement of the model is to simulate the complete three-dimensional geometry. This would allow for the inclusion of heat transfer structures that are immersed into the PCM to enhance heat transfer in the simulation.

The next step is to simulate a series of varying enclosure sizing to further analyze the relationship between sizing and heat transfer mechanism. This is an important preliminary work for the design of future LHTES systems containing rectangular enclosures. With the resulting knowledge, the systems may be specifically adjusted to the requirements of different applications. Also, data from such a parameter study is intended to adjust and validate a self-tailored approach that incorporates a simplified model of natural convection and is able to deliver solutions much faster than the CFD-approach.

6. Acknowledgements

The authors thank the German Federal Ministry for the Environment, Nature Conservation and Nuclear Safety for the financial support given to the DSG-Store project (Contract No. 0325333A).

7. References

[1] Mehling H., Cabeza L. F. Heat and cold storage with PCM. Springer Verlag, Berlin Heidelberg, 2008.

[2] Fiss M. Wärmespeichervorrichtung , Deutsches Patent- und Markenamt, DE 10 2011 001 883 A1 2012.10.11, filed April 7, 2011 and disclosed October 11, 2012.

[3] Johnson M., Fiss M., Klemm T., Eck M., Test and analysis of a flat plate latent heat storage design, in *ISES Solar World Congress*, 2013.

[4] Shatikian V., Ziskind G., Letan R. Numerical investigation of a PCM-based heat sink with internal fins. *Int. J. Heat Mass Transf. 2005;*48(17):3689–3706.

[5] Elder J. Laminar free convection in a vertical slot. *J. Fluid Mech 1965;* 23:77–98.

[6] ANSYS Inc, "ANSYS Fluent User's Guide." 2012.

[7] Voller V., Prakash C. A fixed grid numerical modelling methodology for convection-diffusion mushy region phase-change problems. *Int. J. Heat Mass Transf.* 1987.

[8] Brent A., Voller V., Reid K. Enthalpy-Porosity technique for modeling convection-diffusion phase change: Application to the melting of a pure metal. *Numer. Heat Transf. Part A 1988;* 37–41.